Detached cataclysmic variables are crossing the orbital period gap

M. Zorotovic, M. Schreiber, S. Parsons, B. Gänsicke, A. Hardy, C. Agurto-Gangas, A. Nebot Gómez-Morán, A. Rebassa-Mansergas, A. Schwope

Monthly Notices
of the
ROYAL ASTRONOMICAL SOCIETY

MNRAS **457,** 3867–3877 (2016)
Advance Access publication 2016 January 29

doi:10.1093/mnras/stw246

Detached cataclysmic variables are crossing the orbital period gap

M. Zorotovic,[1⋆] M. R. Schreiber,[1,2] S. G. Parsons,[1] B. T. Gänsicke,[3] A. Hardy,[1] C. Agurto-Gangas,[1,4] A. Nebot Gómez-Morán,[5] A. Rebassa-Mansergas[6] and A. D. Schwope[7]

[1]*Instituto de Física y Astronomía, Universidad de Valparaíso, Av. Gran Bretaña 1111 Valparaíso, Chile*
[2]*Millennium Nucleus 'Protoplanetary Disks in ALMA Early Science', Universidad de Valparaíso, Av. Gran Bretaña 1111 Valparaíso, Chile*
[3]*Department of Physics, University of Warwick, Coventry CV4 7AL, UK*
[4]*Max-Planck-Institut fur extraterrestrische Physik, Giessenbachstrasse 1, D-85748 Garching, Germany*
[5]*Observatoire Astronomique de Strasbourg, Université de Strasbourg, CNRS, UMR 7550, 11 rue de l'Université, F-67000 Strasbourg, France*
[6]*Departament de Física, Universitat Politècnica de Catalunya, c/Esteve Terrades 5, E-08860 Castelldefels, Spain*
[7]*Leibniz-Institut für Astrophysik Potsdam (AIP), An der Sternwarte 16, D-14482 Potsdam, Germany*

Accepted 2016 January 27. Received 2016 January 26; in original form 2015 December 14

ABSTRACT

A central hypothesis in the theory of cataclysmic variable (CV) evolution is the need to explain the observed lack of accreting systems in the ≃2–3 h orbital period range, known as the *period gap*. The standard model, disrupted magnetic braking (DMB), reproduces the gap by postulating that CVs transform into inconspicuous detached white dwarf (WD) plus main sequence systems, which no longer resemble CVs. However, observational evidence for this standard model is currently indirect and thus this scenario has attracted some criticism throughout the last decades. Here, we perform a simple but exceptionally strong test of the existence of detached CVs (dCVs). If the theory is correct, dCVs should produce a peak in the orbital period distribution of detached close binaries consisting of a WD and an M4–M6 secondary star. We measured six new periods which brings the sample of such binaries with known periods below 10 h to 52 systems. An increase of systems in the ≃2–3 h orbital period range is observed. Comparing this result with binary population models, we find that the observed peak cannot be reproduced by post-common envelope binaries (PCEBs) alone and that the existence of dCVs is needed to reproduce the observations. Also, the WD mass distribution in the gap shows evidence of two populations in this period range, i.e. PCEBs and more massive dCVs, which is not observed at longer periods. We therefore conclude that CVs are indeed crossing the gap as detached systems, which provides strong support for the DMB theory.

Key words: Binaries: close – stars: evolution – stars: low-mass – novae, cataclysmic variables – white dwarfs.

1 INTRODUCTION

Cataclysmic variables (CVs) are close binaries in which a main-sequence (MS) donor transfers mass to a white dwarf (WD). The evolution of CVs is driven by angular momentum loss due to gravitational radiation (GR) and the much stronger magnetic braking (MB). The observed orbital period distribution of CVs has an apparent lack of systems in the ≃2–3 h orbital period range, known as the *period gap*. In order to explain this deficit, Rappaport, Joss & Verbunt (1983) proposed a disrupted magnetic braking (DMB) scenario assuming that MB turns off when the donor star becomes fully convective at $P_{\rm orb} \simeq 3$ h. Systems above the gap are driven closer due to GR and efficient MB. Due to the strong mass transfer caused by MB the donors are driven out of thermal equilibrium. Once the donor star becomes fully convective, at the upper edge of the gap, MB stops or at least becomes inefficient. This causes a drop in the mass-transfer rate, which allows the donor star to relax to a radius which is smaller than its Roche lobe radius. The system detaches, mass transfer stops and it becomes a detached WD plus MS (WD+MS) binary, evolving towards shorter periods only via GR. At $P_{\rm orb} \simeq 2$ h the Roche lobe has shrunk enough to restart mass transfer and the system appears again as a CV at the lower edge of the gap.

The DMB scenario not only explains the period gap, but also agrees well with several other observed characteristics of CVs. The

⋆ E-mail: mzorotovic@dfa.uv.cl

model adequately reproduces the higher accretion rates of systems above the period gap (Townsley & Bildsten 2003; Townsley & Gänsicke 2009) and the larger radii of donor stars in CVs above the gap with respect to their MS radii (Knigge, Baraffe & Patterson 2011). In addition, there is evidence for a discontinuity in the braking of single stars (Bouvier 2007; Reiners & Basri 2008) and/or a change in the field topology (Reiners & Basri 2009; Saunders et al. 2009) around the fully convective boundary. Also in wide WD+MS binaries a significant increase in the activity fraction of M-dwarfs at the fully convective boundary has been observed (Rebassa-Mansergas, Schreiber & Gänsicke 2013), which supports the idea that fully convective stars in wide binaries are not spun down as quickly as earlier M-dwarfs. Finally, the prediction of the DMB scenario of a steep decrease of the number of post-common envelope binaries (PCEBs) at the fully convective boundary (Politano & Weiler 2006) is in agreement with the observations (Schreiber et al. 2010).

However, these pieces of evidence supporting the standard theory of CV evolution based on the DMB scenario are rather indirect and the hypothesis that CVs are really crossing the gap as detached systems has been frequently challenged (e.g. Clemens et al. 1998; Andronov, Pinsonneault & Sills 2003; Ivanova & Taam 2003). In addition, the standard scenario for CV evolution is facing several major problems, the most severe being that the predicted WD masses in CVs are systematically smaller than the observed ones (Zorotovic, Schreiber & Gänsicke 2011a). Schreiber, Zorotovic & Wijnen (2016) recently suggested a revision of the standard model of CV evolution incorporating an empirical prescription for consequential angular momentum loss (CAML), i.e. angular momentum loss generated by mass transfer, and showed that the WD mass problem and several others can be solved if CAML is assumed to increase as a function of decreasing WD mass.

A direct test of the main prediction of the standard scenario of CV evolution has been suggested by Davis et al. (2008): if MB is disrupted at the upper boundary of the gap causing CVs to stop mass transfer, these systems should show up in population studies of detached WD+MS binaries. In particular, the deficit of CVs in the $\simeq$2–3 h orbital period range should imply an excess of short-period detached WD+MS binaries in the same period range. Observationally identifying this peak would provide clear evidence for the standard theory of CV evolution and may even allow to distinguish between the classical standard model and the revised version by Schreiber et al. (2016) as the latter predicts the CVs crossing the gap to contain more massive WDs.

We here present the results of an observational search for close detached WD+MS binaries testing if the predicted peak at orbital periods of $\simeq$2–3 h exists. Comparing the observational results with those predicted by binary population models, we find that the existence of detached CVs (dCVs) is required to reproduce the observations, and we therefore conclude that indeed CVs are crossing the gap as detached systems. In addition, as predicted by the revised model proposed by Schreiber et al. (2016), the observed WD mass distribution of detached systems in the $\simeq$2–3 h period range shows evidence for a combined population of PCEBs and dCVs (more massive) in the period gap.

2 THE SPECTRAL TYPES OF dCVs

If the standard theory of CV evolution is correct and CVs are crossing the $\simeq$2–3 h gap as detached systems, a peak of systems should show up in the orbital period distribution of detached PCEBs with secondary stars of spectral types that are expected for dCVs. dCVs should have secondary stars with similar spectral types across the entire period gap, because MB is assumed to stop when the secondary star becomes fully convective and the mass remains constant while they are detached within the gap. Single M-dwarf becomes fully convective at $M_{\rm sec} \simeq 0.35$ M$_\odot$ (Chabrier & Baraffe 1997) which corresponds to a spectral type of M3–M4 (Rebassa-Mansergas et al. 2007). However, in most CVs above the period gap the spectral type of the secondary star is significantly later than the spectral type expected for a zero-age MS star with the same mass (e.g. Baraffe & Kolb 2000). The mass at which a mass-losing star becomes fully convective is smaller than for single stars or secondary stars in detached systems. Using observational constraints from a large sample of CVs, Knigge (2006) find the fully convective boundary for CVs to be at $M_{\rm sec} = 0.2 \pm 0.02$ M$_\odot$, which according to Rebassa-Mansergas et al. (2007) corresponds to a spectral type of $\sim$M6. However, the exact mass at which a CV secondary star becomes fully convective will differ from system to system. For example, it is affected by the time the system spent as a CV before reaching the fully convective boundary. If it started mass transfer very close to the upper edge of the period gap, with the secondary being close to fully convective, the secondary star may be only slightly out of thermal equilibrium when becoming fully convective compared to a system with a longer mass transfer history. This implies that dCVs may cover a range of secondary masses with $M_{\rm sec} \sim 0.2$–0.35 M$_\odot$ which roughly corresponds to spectral types later than $\sim$M4–M6 according to Rebassa-Mansergas et al. (2007). This fits with the spectral-type range for PCEBs that start mass transfer within the period gap if we use the mass spectral-type relation from Rebassa-Mansergas et al. (2007) for detached systems. Therefore, we decided to search for the peak produced by dCVs in the orbital period distribution of a large and unbiased sample of close detached WD+MS binaries with secondaries of spectral type M4–M6 assuming an uncertainty of half a subclass.

However, we are aware of the fact that spectral types of dCVs as well as spectral-type mass and spectral-type radius relations are notoriously uncertain. Therefore, we performed several tests moving the spectral-type range assumed for dCVs one class towards earlier/later spectral types and find that the conclusions of this paper remain identical.

3 THE OBSERVED SAMPLE

In what follows we describe our observational sample. We also present the details of the observations, data reduction and period determination for six systems. We analysed the observed orbital period distribution and the possible biases that affect our sample.

3.1 Systems from the SDSS PCEB survey

Our observational sample is mostly based on the results of a large project we performed over the last decade. The Sloan Digital Sky Survey (SDSS) sample of spectroscopically identified WD+MS binary stars (Rebassa-Mansergas et al. 2012) contains 2316 systems up to data release 8. The majority ($\sim$3/4) of these systems are wide binaries that never underwent a common envelope (CE) event (Schreiber et al. 2010; Nebot Gómez-Morán et al. 2011; Rebassa-Mansergas et al. 2011). We carried out a radial velocity (RV) survey to identify the PCEBs within the SDSS sample (Schreiber et al. 2010), and measured their orbital periods to constrain theories of close binary evolution (Nebot Gómez-Morán et al. 2011). The target selection during this large observational project was mostly determined by observing constraints and otherwise random, i.e. was

mostly independent of the secondaries spectral type. Only in a few cases we targeted systems with a certain spectral type, e.g. when we were trying to measure the increase of systems across the fully convective boundary we preferentially observed systems with M2–M4 secondary stars.

The close binaries discovered in the above described project containing M4–M6 secondary stars with orbital periods measured through RVs or from ellipsoidal/reflection effect (25) are complemented with 22 eclipsing systems identified by combining our spectroscopic WD+MS identification from SDSS with photometry from archival Catalina Sky Survey data (Drake et al. 2010; Parsons et al. 2013a, 2015). This way we established a sample of 47 PCEBs with an orbital period below 10 h and companions with spectral types M4–M6.

We also included in our sample 11 systems with earlier spectral types (M2–M3) and orbital periods below 10 h, selected in the same way, as a control group. We do not expect to see any detached systems in the period gap for this control group, because PCEBs with companions in this spectral-type range should start mass transfer at longer periods.

3.2 VLT/FORS survey of dCVs

To complement the sample that extracted from previous surveys, we carried out a dedicated search of close WD+MS systems with M4–M6 companions to search for dCVs crossing the gap. We measured six periods, five of them shorter than 10 h. This brings our sample size to 52. In the following, we describe the observations and data reduction.

We selected six systems from our catalogue of WD+MS binaries and observed them with the Very Large Telescope (VLT) UT1 equipped with the Focal Reducer and low dispersion Spectrograph (FORS2; Appenzeller et al. 1998) on the nights of 2014 May 16–18 and 2015 July 2–4, in order to determine their orbital periods. We used the long slit mode with a 0.7 arcsec slit, 2 × 2 binning, the 1028z grism and the OG590 filter, resulting in a wavelength coverage of 7700–9500 Å with a dispersion of 0.8 Å pixel^{-1}. The data were reduced using the standard European Southern Observatory (ESO) reduction pipeline. We also applied a telluric correction to the data using observations of the DQ WD GJ 440 taken at the start of each night. We measured the RV of the M dwarf in each spectrum by fitting the Na I absorption doublet at ∼8200 Å with a combination of a straight line and two Gaussians of fixed separation, typically reaching a precision of 5–10 km s^{-1} in each individual spectrum. We then determined the orbital periods of the binaries by fitting a constant plus sine wave to the velocity measurements over a range of periods and computing the χ^2 of the resulting fit. In Fig. 1, we show the phase-folded RV curves and corresponding fits for these systems. Table 1 lists the results of these fits and the parameters of the systems, where the WD temperatures and masses are taken from Rebassa-Mansergas et al. (2012) and 3D model corrections have been applied for systems with temperatures below 12 000 K (Tremblay et al. 2013). SDSS J1452+2045 and SDSS J2208+0037 show no absorption features from the WD in the SDSS spectra, meaning that the masses and temperatures cannot be reliably determined. However, the RV semi-amplitude can be used to determine a lower limit on the WD mass, which is provided in Table 1.

3.3 Observed period distribution

Our final sample contains 52 close WD+MS binaries with orbital periods $P_{\rm orb} \leq 10$ h and spectral types M4–M6. Their parameters as well as an explanation of how the close binary nature has been revealed and how the period has been measured are listed in Table A1 in the Appendix. The masses and temperatures of WDs cooler than 12 000 K have been updated based on 3D model corrections (Tremblay et al. 2013) except in some systems where the inclination is constrained by the eclipse which places a limit on the WD mass that is more accurate than the mass estimated from the spectra.

The left-hand panel in Fig. 2 shows the observed orbital period distribution of close detached WD+MS binaries in our sample with secondary stars in the spectral-type range M4–M6 (top) and M2–M3 (bottom). The hatched area corresponds to the period gap according to Knigge (2006). The binning has been chosen to cover the whole gap in only one bin (2.15–3.18 h). A peak can be observed at the position of the period gap for systems containing M4–M6 companions. On the other hand, the period distribution of PCEBs with secondaries in the spectral-type range M2–M3 only contains systems with periods above the gap. This confirms that we have selected the correct spectral-type range to search for dCVs and that our results are not affected by the uncertainty of the spectral type of the secondary star, which is typically roughly half a subclass (Rebassa-Mansergas et al. 2007).

3.4 Possible observational biases

The close WD+MS binaries in our sample have been identified through RV variations or eclipses in their light curves. Both methods imply an observational bias towards short orbital periods that we have to consider before comparing the observed period distribution with the results of binary population models.

Systems with shorter periods show larger RV variations and therefore their close nature is easier to determine. However, as shown in Nebot Gómez-Morán et al. (2011, their fig. 10), the detection probability of close binarity only significantly decreases at periods longer than about one day. Therefore, for the majority of systems (35) in our sample which have been identified as close binaries through RV measurements, we can clearly exclude observational biases to affect our results.

Eclipse light curves led to the discovery of the close binary nature in 17 systems in our sample. As shown by Parsons et al. (2013a), the baseline and cadence of the archival Catalina data is typically good enough to detect eclipsing systems with orbital periods of about a day, so the detection probability again should not affect our results. However, the detection probability is not the only possible bias towards shorter periods in the case of eclipses. The smaller the orbital period, the wider the range of inclinations that produce an eclipse. In other words, there is a larger fraction of eclipsing systems at shorter orbital periods. This has been shown in Parsons et al. (2013a, fig. 4), where a comparison between the period distribution of all SDSS spectroscopically confirmed eclipsing PCEBs and all SDSS PCEBs from Nebot Gómez-Morán et al. (2011) has been performed. To test whether the latter bias could affect our results, we investigated the fraction of eclipsing systems in our observational sample and found that 40 per cent of the systems with M4–M6 companions are known to be eclipsers: 50 per cent of the systems in the period gap and 38 per cent above (see Table A1 in the Appendix). This confirms that the fraction of eclipsing systems is larger in the bin with the shortest periods, although we cannot exclude that this is caused by the low number of systems. Also, in some of these systems their close nature was initially revealed from RV variations and their eclipsing nature was subsequently discovered. We found that the fraction of systems that were discovered to be close solely due to their eclipsing nature is similar in the gap and outside (33 per cent

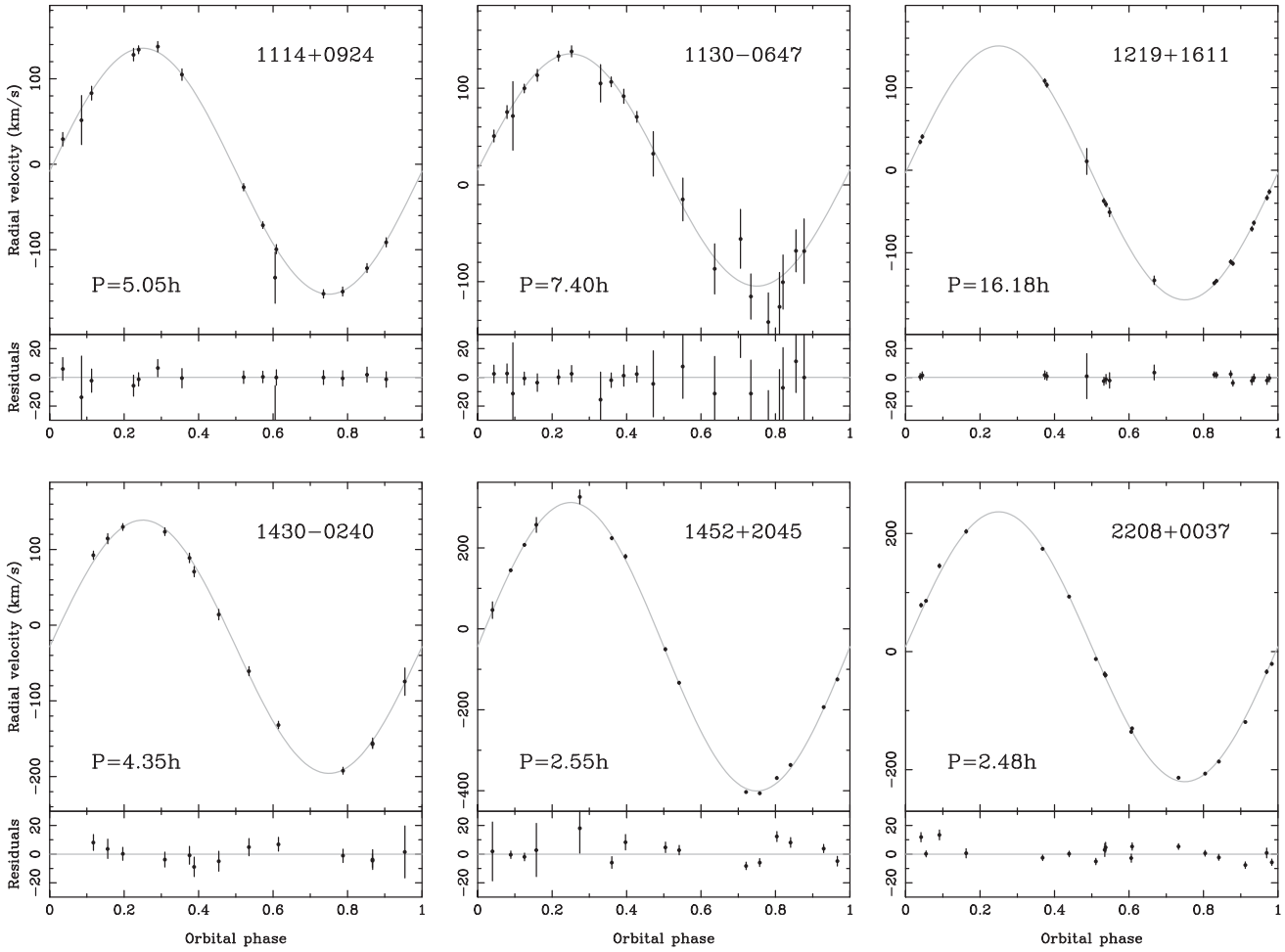

Figure 1. Phase-folded RV curves for the six systems with periods presented in this paper. The grey line in each panel shows the sine fit to the data (see Table 1 for more details). The panel below each RV curve shows the residuals to this fit.

Table 1. Six SDSS WD+MS binaries with new orbital period measurements. Uncertainties in the periods are given in parentheses.

System	$P_{\rm orb}$ (d)	γ (km s^{-1})	K_2 (km s^{-1})	$T_{\rm eff}$ (K)	$M_{\rm WD}$ ($M_\odot$)	Sp2
SDSS J111459.93+092411.0	0.210 2534(1)	-8.2 ± 1.6	143.9 ± 2.1	$10\,324 \pm 172$	0.610 ± 0.115	M5
SDSS J113006.11−064715.9	0.308 5042(7)	15.5 ± 3.6	120.1 ± 4.8	$11\,139 \pm 192$	0.520 ± 0.076	M5
SDSS J121928.05+161158.7	0.674 080(1)	-3.2 ± 0.9	153.8 ± 1.4	7123 ± 103	0.930 ± 0.124	M6
SDSS J143017.22−024034.1	0.181 409 00(9)	-28.5 ± 1.7	167.4 ± 2.1	$10\,802 \pm 436$	0.640 ± 0.201	M5
SDSS J145238.12+204511.9	0.106 218 03(3)	-44.1 ± 1.1	356.5 ± 1.4	–	$\geq$0.89	M4
SDSS J220848.32+003704.6	0.103 351(9)	8.3 ± 0.7	228.4 ± 1.0	–	$\geq$0.33	M5

and 30 per cent, respectively). This means that the potential bias towards shorter periods caused by close systems identified through eclipses is not important and cannot be responsible for the peak observed at the position of the period gap in the upper-left panel of Fig. 2.

While we can exclude that our sample is significantly biased with respect to the orbital period, the situation is different concerning the temperature of the WDs in our systems. If the WD is colder than ∼8000 K it becomes very difficult to measure its temperature from SDSS spectra, because no hydrogen absorption lines are present, which leads to a clear bias against old systems. The two systems in our observed sample with WD temperatures significantly below 8000 K (SDSS J0138−0016 and SDSS J1210+3347) are eclipsing and the WD temperatures were determined from their colours. This bias against systems containing cold WDs has to be taken into account when comparing observed and simulated populations.

Finally, given the importance of the WD mass for our understanding of CV evolution, we consider possible biases affecting this parameter. The RV method for identifying close binaries causes a bias towards systems with larger WD masses because, for a given secondary mass and orbital period, the velocity of the secondary increases with WD mass. This bias does not affect the relative distribution of WD masses as it is independent of the orbital period (i.e. each orbital period bin is equally biased). In the case of eclipsing systems, the identification probability is virtually independent of the WD mass.

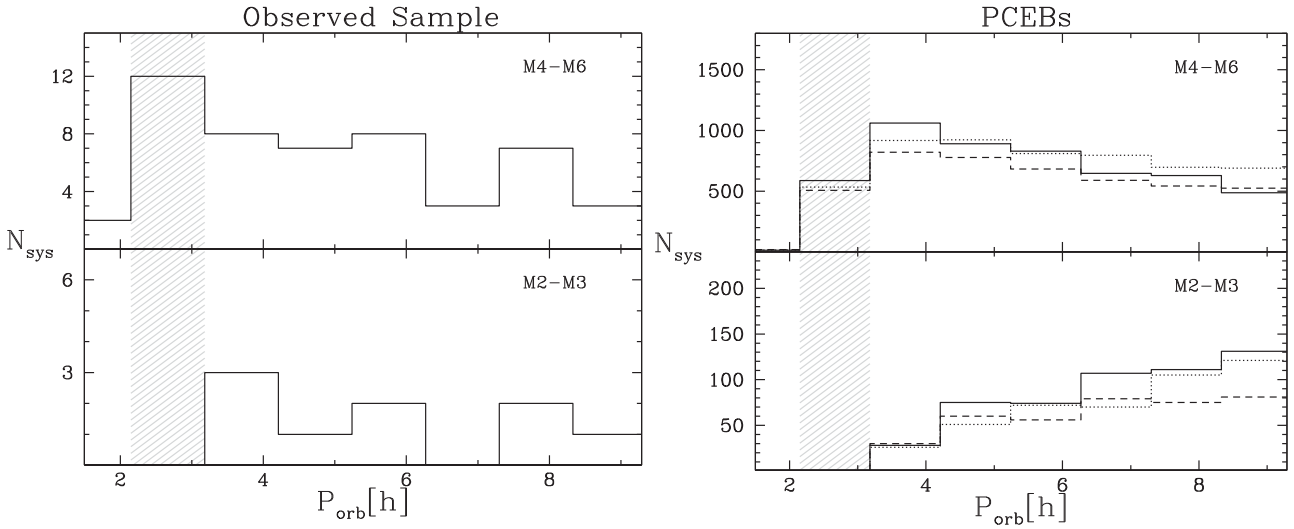

Figure 2. Left: observed period distribution for detached WD+MS binaries. The upper and bottom panels show the distribution for different ranges of spectral types for the MS companion. The corresponding ranges are labelled in the top-right corner of each panel. The hatched area represents the location of the period gap (2.15–3.18 h, Knigge 2006). Right: orbital period distribution for the simulated population of PCEBs with secondary stars in the corresponding spectral-type ranges. The solid line corresponds to the simulations with $\alpha_{\rm CE} = 0.25$, the dotted line to $\alpha_{\rm CE} = 0.5$, and the dashed line to $\alpha_{\rm CE} = 1.0$.

4 BINARY POPULATION MODELS

The observed period distribution of close but detached WD+MS systems with secondary spectral types of M4–M6 shows a peak at the position of the orbital period gap. In order to evaluate if this peak provides evidence for CVs crossing the gap as detached system, we performed Monte Carlo simulations of the population of WD+MS PCEBs and dCVs in the period gap. In what follows we describe the details of our population models.

4.1 PCEBs

An initial MS+MS binary population of 10^7 systems was generated. We assumed the initial mass function of Kroupa, Tout & Gilmore (1993) in the range 0.8–9 $M_\odot$ for the distribution of primary masses plus a flat initial mass-ratio distribution (Sana, Gosset & Evans 2009) for secondary masses, with a lower limit of $M_{\rm sec} = 0.05\ M_\odot$. A flat distribution in $\log a$ ranging from 3 to 10^4 $R_\odot$ was used for the orbital separations (Popova, Tutukov & Yungelson 1982; Kouwenhoven et al. 2009) and a constant star formation rate was assumed with an upper limit of 10 Gyrs.

As in Schreiber et al. (2016), the systems were first evolved until the end of the CE phase using the binary-star evolution (BSE) code from Hurley, Tout & Pols (2002). Three different values of the CE efficiency were considered: $\alpha_{\rm CE} = 0.25$, $\alpha_{\rm CE} = 0.5$, and $\alpha_{\rm CE} = 1.0$. The subsequent evolution of these zero-age PCEBs was performed with our own code. All zero-age PCEBs were evolved to their current periods assuming systemic angular momentum loss due to MB and GR (if $M_{\rm sec} > 0.35\ M_\odot$) or GR only (if $M_{\rm sec} \leq 0.35\ M_\odot$). The normalization factors for MB and GR are based on the observational constraints derived by Knigge et al. (2011). If a system filled its Roche lobe it was not considered as a PCEB anymore.

The spectral-type range of the MS star was converted into a mass range based on the relation presented in Rebassa-Mansergas et al. (2007). The range M4–M6 corresponds to masses for the companion in the range 0.17–0.35 $M_\odot$, which is consistent with the mass range used by Davis et al. (2008). Furthermore, this corresponds to the mass range of secondary stars that will commence mass transfer within the gap. PCEBs in this mass range are assumed to evolve towards shorter periods due to GR only. The spectral-type range M2–M3 used for comparison corresponds to a mass range of 0.35–0.45 $M_\odot$ for the companion. These systems are brought into contact mainly due to MB and therefore evolve faster towards a second mass transfer phase. These systems will start the second mass transfer phase at periods above the gap and therefore we do not expect to see any such system within the gap.

4.2 Cataclysmic variables

To estimate the impact of dCVs on the predicted population of close detached systems with secondary spectral types of M4–M6, we extended the binary population synthesis model described above by incorporating CV evolution following Schreiber et al. (2016). Once the secondary star fills its Roche lobe it is inflated to a larger radius based on the mass–radius relation for CVs above the gap given by Knigge et al. (2011). We stop MB when the secondary star reaches 0.2 $M_\odot$ and the system becomes a dCV which evolves through the period gap only via GR.

As shown in Schreiber et al. (2016), the simulated population of CVs is strongly affected by the critical mass ratio that is assumed for having stable mass transfer. Apart from the intrinsic angular momentum loss due to GR and MB, CAML, i.e. angular momentum loss due to mass transfer and mass-loss during the nova eruptions, can play an important role. Two different models for CAML are simulated: the classical non-conservative model for CAML (cCAML) where the change in angular momentum is given by

$$\frac{\dot{\rm J}_{\rm CAML}}{\rm J} = \frac{{M_{\rm sec}}^2}{M_{\rm WD}(M_{\rm WD} + M_{\rm sec})} \frac{\dot{\rm M}_{\rm sec}}{M_{\rm sec}} \quad (1)$$

(see e.g. King & Kolb 1995), and an empirical CAML (eCAML) model given by

$$\frac{\dot{\rm J}_{\rm CAML}}{\rm J} = \frac{0.35}{M_{\rm WD}} \frac{\dot{\rm M}_{\rm sec}}{M_{\rm sec}} \quad (2)$$

(Schreiber et al. 2016) that recently has shown to solve several problems between predictions and observations of CVs, especially the disagreement between observed and predicted WD masses. In

the eCAML model, we adjusted the normalization factors for MB and GR in order to obtain mass transfer rates in CVs that are consistent with the ones obtained with the cCAML model. The factors we used are 0.43 for MB and 1.67 for GR (instead of 0.66 and 2.74, respectively, from Knigge et al. 2011). This means that systems evolve slower towards shorter periods when there is no mass transfer. However, as the star formation rate is constant and we do not take into account old (cool) systems, these factors should not affect the orbital period distribution for the PCEB population. The spectral-type mass conversion was performed as in the case of PCEBs.

5 COMPARISON WITH THE OBSERVATIONS

To compare the simulated populations with the observations, we excluded systems with old WDs that are too cool to be reliably detected through observations, because the observed sample is strongly biased against such systems. The detectability of a WD against a companion of the same spectral type depends mostly on the WD effective temperature and only little on its mass (Zorotovic et al. 2011a). Therefore, applying a temperature limit of 8000 K to all our systems seems reasonable for comparing observed and simulated populations. We estimated the effective temperature of the WDs using the cooling tracks by Althaus & Benvenuto (1997)[1] for helium-core WDs (if $M_{\rm WD} \lesssim 0.5$ M$_\odot$) and Fontaine, Brassard & Bergeron (2001)[2] for carbon/oxygen-core WDs (if $M_{\rm WD} \gtrsim 0.5$ M$_\odot$). The temperatures of the WDs in PCEBs and dCVs were calculated in the same way. We note that the effective temperature of the WD in a dCV might be affected by compressional heating during the previous CV phase (Sion 1995; Townsley & Bildsten 2004; Townsley & Gänsicke 2009). However, it is not clear how long it takes for the WD to cool down after mass transfer stops. If the time-scale is longer or comparable to the time a dCV spends in the gap, i.e. if the effective temperature of a dCV is higher than the cooling temperature, the number of dCVs produced by the simulations can be slightly underestimated.

We start our comparison by using PCEBs only to test if the peak observed at the position of the period gap for systems with M4–M6 companions can be reproduced without assuming dCVs crossing the gap.

5.1 PCEBs

In the right-hand panel of Fig. 2, we show the simulated orbital period distribution for PCEBs. The different lines correspond to different values of the CE efficiency. The upper panel, which contains systems with M4–M6 secondary stars, shows a trend to have more systems towards shorter periods with a drop in the period gap, independent of the CE efficiency parameter. In contrast, the bottom panel shows a decrease of systems with M2–M3 secondary stars towards shorter periods and none within the gap. This is expected because systems with earlier spectral types have more massive secondaries that fill their Roche lobes at longer periods.

While the observed and predicted distributions for systems with M2–M3 secondary stars agree quite well in not showing any system within the gap (and keeping in mind that the observed sample is admittedly small), the observed peak at the period gap for systems with spectral types M4–M6 is in contrast to the drop expected from our simulations of the PCEB population if dCVs do not exist. In the next section, we evaluate if this is better reproduced if we include dCVs.

5.2 Including dCVs

Fig. 3 shows the simulated orbital period distribution for the combined population of PCEBs and dCVs in the same spectral-type ranges as in Fig. 2. As expected, the distributions of the systems with M2–M3 secondaries (bottom panels) do not change because no detached systems with M2–M3 secondaries are produced by CV evolution. The difference between the distributions in the left-hand and right-hand panels in this range is purely due to the normalization factors for MB and GR assumed in each model.

The predicted orbital period distributions for close detached systems with secondaries of spectral type M4–M6, however, are significantly affected. The number of systems in the orbital period range of the period gap is clearly increased. This effect is strongest for small values of $\alpha_{\rm CE}$ and stronger in the cCAML model than in the eCAML model. Comparing with the observed distribution (Fig. 2, left-hand panel) it seems that especially models assuming small values for $\alpha_{\rm CE}$ provide a better agreement between theory and observations than is reachable with PCEBs alone.

However, given the still relatively low number of systems in our sample, we need to carefully investigate whether this apparent improvement provides statistically robust evidence for the existence of dCVs crossing the gap. To that end, we performed a Kolmogorov–Smirnov (KS) test between the observed and simulated period distributions. Fig. 4 shows the cumulative distributions of orbital periods for our simulations (black) and the observed systems (red) with MS companions in the spectral-type range M4–M6. The left-hand panel compares the observational sample with our PCEB simulations (without dCVs), middle shows the comparison with PCEBs + dCVs from the cCAML model, and the right-hand panel compares observations with PCEBs + dCVs from the eCAML model. Different styles of lines correspond to the three different CE efficiencies used in the simulations. The KS probabilities are also listed in the upper-left corner of each panel. According to the KS test, the cumulative distribution of observed systems and PCEBs is different with a confident level of at least 98.4 per cent depending on the value of the CE efficiency that is assumed. The corresponding KS probability is less than 0.02 and we therefore conclude that the two samples are different. In the case of PCEBs + dCVs, both models show larger KS probabilities when a small CE efficiency is assumed ($\alpha_{\rm CE} = 0.25$). For the cCAML model the KS probability is 0.670 while for the eCAML it is 0.234. Based on these values, we cannot exclude any of the two models. However, the probabilities drop dramatically if we use larger values for the CE efficiency and all the models with $\alpha_{\rm CE} = 0.5$ or $\alpha_{\rm CE} = 1.0$ can be rejected with a confidence level larger than 98 per cent. This is consistent with recent studies that show that low values of $\alpha_{\rm CE}$ seem to work best for PCEBs with M-dwarf secondaries (e.g. Zorotovic et al. 2010; Toonen & Nelemans 2013; Camacho et al. 2014). We also performed the KS tests for the simulated and observed systems with secondary stars in the spectral-type range M2–M3. Comparing with the predicted PCEB sample the KS probabilities are larger than 0.1 for both CAML models and for the three values of the CE efficiency assumed in our simulations. This means that there are no statistically significant differences in the two distributions, i.e. observations and predictions agree.

[1] http://fcaglp.fcaglp.unlp.edu.ar/evolgroup/TRACKS/tracks_heliumcore_prev.html
[2] http://www.astro.umontreal.ca/bergeron/CoolingModels

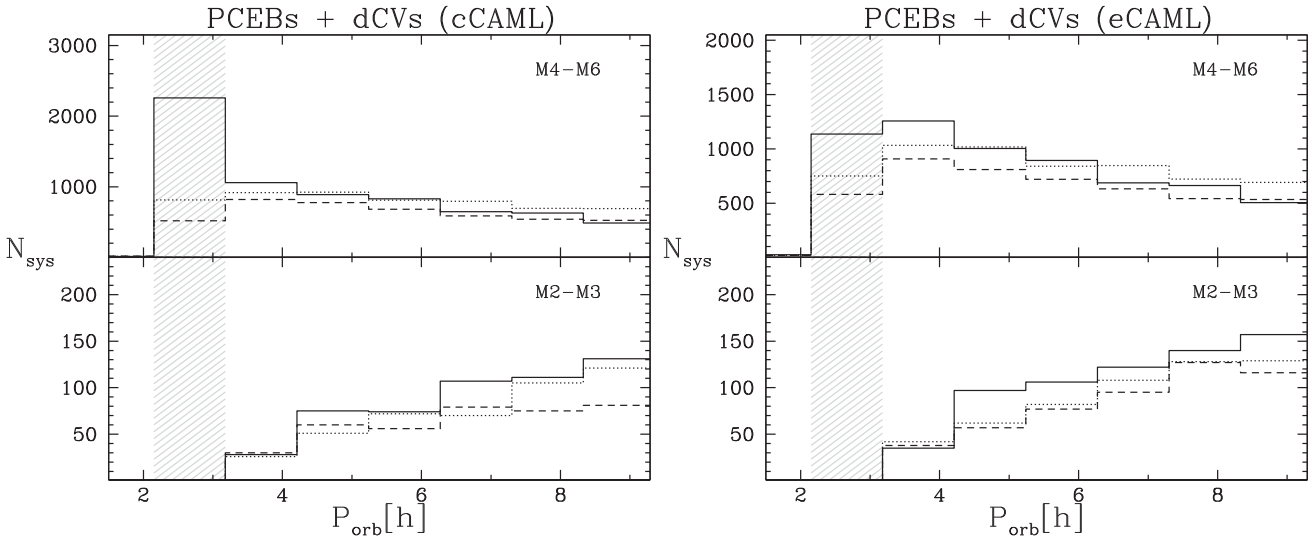

Figure 3. Same as in Fig. 2 but including the population of dCVs in the period gap for our two models: cCAML (left) and eCAML (right). The different styles of lines correspond to different values for the CE efficiency: $\alpha_{CE} = 0.25$ (solid), $\alpha_{CE} = 0.5$ (dotted), and $\alpha_{CE} = 1.0$ (dashed).

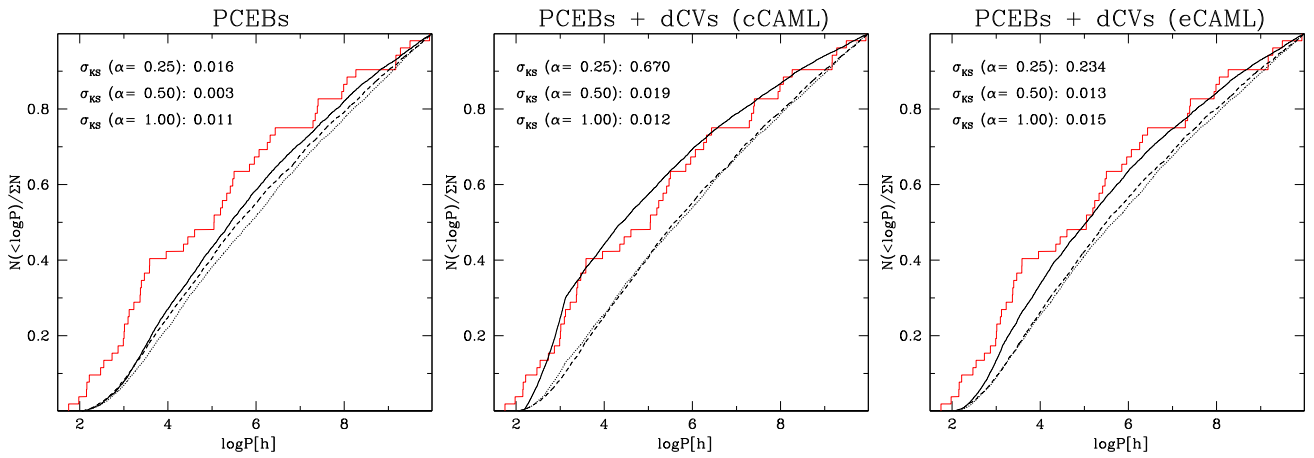

Figure 4. Comparison between the observed (red) and simulated (black) cumulative distribution of orbital periods. Left-hand panel: only PCEBs; middle panel: PCEBs + dCVs from the cCAML model; right-hand panel: PCEBs + dCVs from the eCAML model. The different styles of lines in each panel correspond to different CE efficiencies: $\alpha_{CE} = 0.25$ (solid line), $\alpha_{CE} = 0.5$ (dotted line) and $\alpha_{CE} = 1.0$ (dashed line). The values in the upper-left corner of each panel are the KS probabilities.

6 DISENTANGLING dCVs AND PCEBs

In the previous section, we showed that PCEBs alone cannot be responsible for the observed peak at the position of the period gap in the observed period distribution of detached close WD+MS systems with secondaries of spectral type M4–M6. If there were only PCEBs, one should expect to see a drop in the number of systems in this bin, because PCEBs with secondary stars in this spectral-type range fill their Roche lobes within the gap. The inclusion of dCVs in the gap can reproduce the observed peak, and the size of the expected peak depends strongly on the model that we assume for CAML and on the efficiency for CE ejection. Only with a small value for α_{CE} does the KS test show no significant differences between the observed and simulated distributions with dCVs, in agreement with Zorotovic et al. (2010). Based on the current data, we cannot decide which of the two models for CAML we tested should be preferred as both models produce reasonable agreement with the observations. However, our results clearly show that CVs are crossing the gap as detached systems, which provides further evidence for the DMB model. The question that immediately arises from this result is: is there a way of observationally distinguishing a normal PCEB from a dCV in the period gap? While the secondary stars of dCVs should be indistinguishable from those of PCEBs with M4–M6 secondaries, the WD parameter distributions may provide new insights.

6.1 WD masses

As shown in Zorotovic et al. (2011a), the WD mass distribution of CVs and PCEBs is very different. WDs in CVs are, on average, more massive and there is a lack of low-mass WDs (helium-core WDs). If some of the systems within the period gap are in fact dCVs, one should expect to have a larger average WD mass in this period range than at longer periods.

In Fig. 5, we show the distribution of WD masses and orbital periods for the observed systems with measured WD mass (red dots) and for our simulations assuming $\alpha_{CE} = 0.25$ (grey-scale density). In the simulation that only includes PCEBs (left-hand panel) the

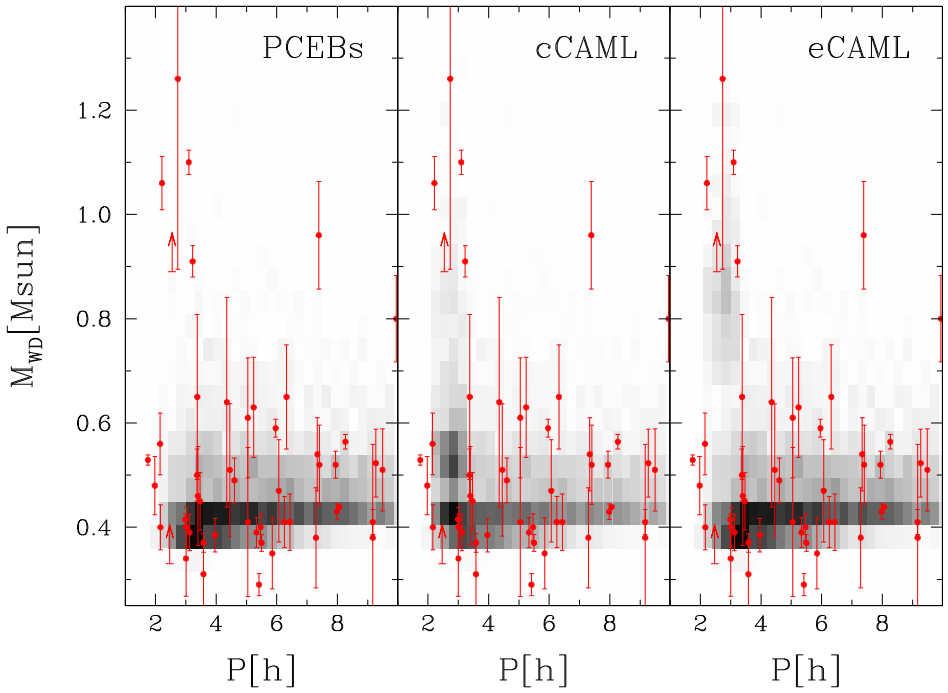

Figure 5. Relation between WD mass and orbital period. The intensity of the grey-scale represents the density of simulated objects in each bin, on a linear scale, and normalized to one for the bin that contains most systems. The red dots are the observed systems with available WD masses. The two vertical arrows correspond to SDSS J1452+2045 and SDSS J2208+0037 for which a lower limit for the WD mass has been calculated based on the RV semi-amplitude.

systems are concentrated at low-mass WDs in all period ranges, exhibiting a single peak (at ∼0.40–0.45 $M_\odot$) and a continuous decrement of systems towards more massive WDs. On the other hand, in our two simulations with dCVs a second population is clearly visible in the ≃2–3 h orbital period range. In the case of the cCAML model (middle panel), a second peak is evident at ∼0.5–0.6 $M_\odot$ and systems with more massive WDs become more frequent at these periods. In the eCAML model, the second peak is not as pronounced as in the cCAML model, but occurs at higher masses (∼0.8–0.9 $M_\odot$). This is because the eCAML model is more restrictive than the cCAML model with respect to the stability limits for mass transfer and therefore produces less CVs (and subsequently less dCVs) but with higher WD masses, which is more consistent with the observed WD mass distribution of CVs.

From the observational sample, we see that the population of systems with massive WDs (>0.8 $M_\odot$) is concentrated at the location of the period gap. We obtain an average WD mass of 0.66 ± 0.12 $M_\odot$ in the gap and 0.50 ± 0.02 $M_\odot$ outside the gap, with standard deviations of 0.35 $M_\odot$ and 0.15 $M_\odot$, respectively, for the systems with M4–M6 companions. This is consistent with having some dCVs with massive WDs in the period gap and seems to provide further support for the eCAML model. However, the tendency of having high-mass WDs in the gap needs to be interpreted with caution because of two reasons: first, our sample is too small to provide a statistically significant result. Secondly, it has been previously found that some of the masses derived from spectra may overestimate significantly the true value, especially if the spectrum is dominated by the MS star component (Parsons et al. 2013a). This is almost certainly the case for SDSS J0052−0053, the system in the gap with the most massive WD (1.26 $M_\odot$). However, for two other gap systems with $M_{\rm WD} > 1$ $M_\odot$, the WD is clearly visible in their SDSS spectra, meaning that these systems quite likely contain massive WDs. One of these systems, SDSS J1013+2724, is in fact an eclipsing system and Parsons et al. (2015) noted that the sharp ingress and egress eclipse features are in agreement with a small (hence massive) WD. The large RV semi-amplitude of SDSS J1452+2045 (one of the new systems presented in this paper) also places a lower limit on the mass of this DC WD of 0.89 $M_\odot$. In summary, there seems to be an excess of systems containing fairly massive WDs with periods in the gap and these may well be dCVs crossing the gap.

6.2 WD effective temperatures

A second possibility to distinguish dCVs and PCEBs might be the effective temperature of the WD. In comparison with CVs above the period gap, dCVs should be cooler because CVs suffer from compressional heating of the outer layers (Sion 1995). On the other hand, dCVs should be hotter than PCEBs in the same orbital period range, because the initial mass of the secondary star must have been higher than the limit for non-fully convective secondaries ($M_{\rm sec} \gtrsim 0.35$ $M_\odot$) in order to start mass transfer above the gap. This means that angular momentum loss after the CE phase was mainly driven by MB. PCEBs in the orbital period range of the period gap, however, need to have less massive secondaries in order to still be detached systems in this period range (≃2–3 h). This means that after the CE phase they become closer only due to GR and therefore they evolve slower towards shorter periods. This effect, however, might be compensated by the fact that systems with more massive companions tend to emerge from the CE phase at slightly longer periods (e.g. Zorotovic et al. 2011b, 2014). Which of the two effects is stronger is uncertain because it depends on, e.g. the initial orbital period, the star formation rate, the CE efficiency or the strength of MB and GR.

Fig. 6 shows the relation between WD effective temperature and orbital period for our simulations with $\alpha_{\rm CE} = 0.25$ (grey-scale

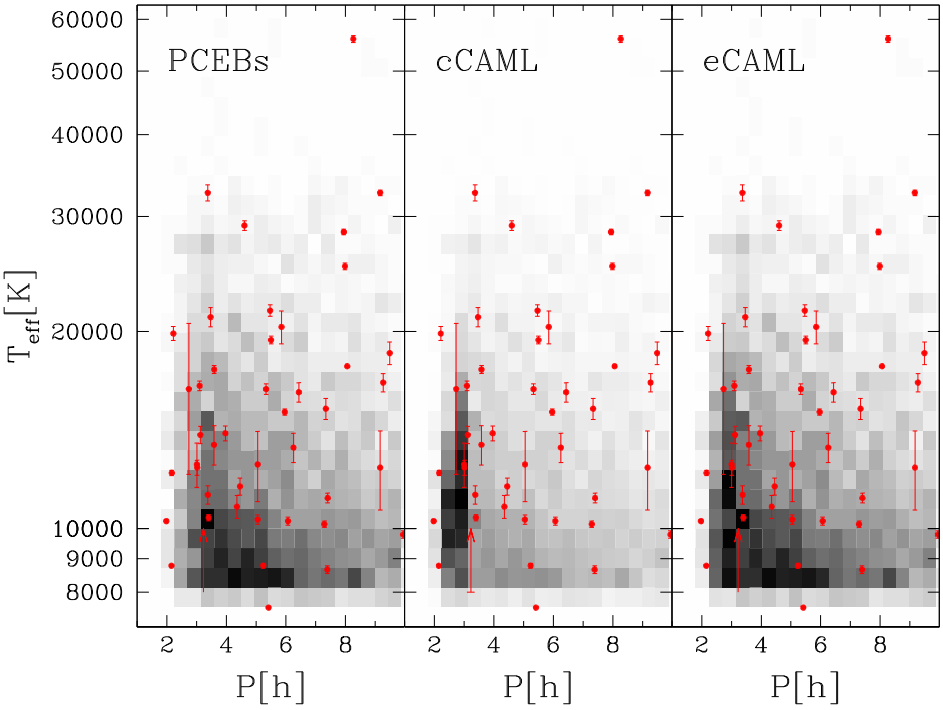

Figure 6. Relation between the WD effective temperature and orbital period. The intensity of the grey-scale for the simulations means the same as in Fig. 5. The red dots are the observed systems with available WD temperatures.

density plot) and for the observed systems with available WD temperatures (red dots). The two observed systems with the lowest temperatures are not represented in this figure because our simulations exclude cold (<8000 K) WDs. The average temperature seems to increase towards shorter periods in all our models and there is no distinctive behaviour at periods corresponding to the period gap. The simulation that only includes PCEBs (left-hand panel) looks almost identical to the one with dCVs from the eCAML model (right-hand panel) while the cCAML model predicts a small increase of the number of hotter WDs in the orbital period range of the gap. This is because this model produces the largest fraction of dCVs compared to PCEBs at these periods. However, in general the predicted distributions of WD temperatures are not significantly different and, in agreement with this, the observed WD temperatures do not show any significant tendency either. The observed WD effective temperature average is $\sim$13 000 $\pm$ 1 300 K in the gap and $\sim$17 000 $\pm$ 1600 K, outside the gap, with standard deviations of $\sim$4000 and $\sim$9500 K, respectively. The dispersion in both, observations and simulations, is substantial. We therefore conclude that the WD temperature is not a suitable parameter to identify dCVs within the period gap.

7 CONCLUSION

We have measured six new periods of close detached WD+MS binaries with secondary stars in the spectral-type range M4–M6, which should correspond to the spectral-type range of secondary stars in dCVs crossing the orbital period gap. These new measurements bring the sample of such binaries with measured orbital period to 52 systems. A clear peak in the orbital period distribution can be observed at the position of the orbital period gap, in agreement with the predictions from the DMB model. Comparing the observed period distribution with the results of binary population models, we find that this peak cannot be explained without assuming that CVs are crossing the gap as detached systems. Therefore, we conclude that indeed CVs become detached binaries at the upper edge of the period gap, which supports the idea that MB becomes inefficient at the fully convective boundary.

We also see clear signs of a different WD mass distribution in the gap and at longer periods. The WD mass distribution of systems within the gap shows a second peak at larger masses which is consistent with having two populations in this period range, i.e. normal PCEBs and the more massive dCVs crossing the gap, in agreement with the model recently proposed by Schreiber et al. (2016).

ACKNOWLEDGEMENTS

We thank Fondecyt for their support under the grants 3130559 (MZ), 1141269 (MRS), and 3140585 (SGP). The research leading to these results has received funding from the European Research Council under the European Union's Seventh Framework Programme (FP/2007-2013)/ERC Grant Agreement no. 320964 (WDTracer). This research was also partially funded by MINECO grant AYA2014-59084-P and by the AGAUR (ARM). The results presented in this paper are based on observations collected at the ESO under programme IDs 093.D-0441 and 095.D-0739.

REFERENCES

Althaus L. G., Benvenuto O. G., 1997, ApJ, 477, 313
Andronov N., Pinsonneault M., Sills A., 2003, ApJ, 582, 358
Appenzeller I. et al., 1998, The Messenger, 94, 1
Baraffe I., Kolb U., 2000, MNRAS, 318, 354
Bouvier J., 2007, in Bouvier J., Appenzeller I., eds, Proc. IAU Symp. 243, Star-Disk Interaction in Young Stars. Cambridge Univ. Press, Cambridge, p. 231

Camacho J., Torres S., García-Berro E., Zorotovic M., Schreiber M. R., Rebassa-Mansergas A., Nebot Gómez-Morán A., Gänsicke B. T., 2014, A&A, 566, A86
Chabrier G., Baraffe I., 1997, A&A, 327, 1039
Clemens J. C., Reid I. N., Gizis J. E., O'Brien M. S., 1998, ApJ, 496, 352
Davis P. J., Kolb U., Willems B., Gänsicke B. T., 2008, MNRAS, 389, 1563
Drake A. J. et al., 2010, preprint (astro-ph/1009.3048)
Fontaine G., Brassard P., Bergeron P., 2001, PASP, 113, 409
Green R. F., Richstone D. O., Schmidt M., 1978, ApJ, 224, 892
Hurley J. R., Tout C. A., Pols O. R., 2002, MNRAS, 329, 897
Ivanova N., Taam R. E., 2003, ApJ, 599, 516
King A. R., Kolb U., 1995, ApJ, 439, 330
Knigge C., 2006, MNRAS, 373, 484
Knigge C., Baraffe I., Patterson J., 2011, ApJ, 194, 28
Kouwenhoven M. B. N., Brown A. G. A., Goodwin S. P., Portegies Zwart S. F., Kaper L., 2009, A&A, 493, 979
Kroupa P., Tout C. A., Gilmore G., 1993, MNRAS, 262, 545
Nebot Gómez-Morán A. et al., 2009, A&A, 495, 561
Nebot Gómez-Morán A. et al., 2011, A&A, 536, A43
Parsons S. G. et al., 2012a, MNRAS, 420, 3281
Parsons S. G. et al., 2012b, MNRAS, 426, 1950
Parsons S. G. et al., 2013a, MNRAS, 429, 256
Parsons S. G., Marsh T. R., Gänsicke B. T., Schreiber M. R., Bours M. C. P., Dhillon V. S., Littlefair S. P., 2013b, MNRAS, 436, 241
Parsons S. G. et al., 2015, MNRAS, 449, 2194
Politano M., Weiler K. P., 2006, ApJ, 641, L137
Popova E. I., Tutukov A. V., Yungelson L. R., 1982, Ap&SS, 88, 55
Pyrzas S. et al., 2009, MNRAS, 394, 978
Pyrzas S. et al., 2012, MNRAS, 419, 817
Rappaport S., Joss P. C., Verbunt F., 1983, ApJ, 275, 713
Rebassa-Mansergas A., Gänsicke B. T., Rodríguez-Gil P., Schreiber M. R., Koester D., 2007, MNRAS, 382, 1377
Rebassa-Mansergas A. et al., 2008, MNRAS, 390, 1635
Rebassa-Mansergas A., Nebot Gómez-Morán A., Schreiber M. R., Girven J., Gänsicke B. T., 2011, MNRAS, 413, 1121
Rebassa-Mansergas A., Nebot Gómez-Morán A., Schreiber M. R., Gänsicke B. T., Schwope A., Gallardo J., Koester D., 2012, MNRAS, 419, 806
Rebassa-Mansergas A., Schreiber M. R., Gänsicke B. T., 2013, MNRAS, 429, 3570
Reiners A., Basri G., 2008, ApJ, 684, 1390
Reiners A., Basri G., 2009, A&A, 496, 787
Sana H., Gosset E., Evans C. J., 2009, MNRAS, 400, 1479
Saunders E. S., Naylor T., Mayne N., Littlefair S. P., 2009, MNRAS, 397, 405
Schreiber M. R., Gänsicke B. T., Southworth J., Schwope A. D., Koester D., 2008, A&A, 484, 441
Schreiber M. R. et al., 2010, A&A, 513, L7
Schreiber M. R., Zorotovic M., Wijnen T. P. G., 2016, MNRAS, 455, L16
Sion E. M., 1995, ApJ, 438, 876
Toonen S., Nelemans G., 2013, A&A, 557, A87
Townsley D. M., Bildsten L., 2003, ApJ, 596, L227
Townsley D. M., Bildsten L., 2004, ApJ, 600, 390
Townsley D. M., Gänsicke B. T., 2009, ApJ, 693, 1007
Tremblay P.-E., Ludwig H.-G., Steffen M., Freytag B., 2013, A&A, 559, A104
Zorotovic M., Schreiber M. R., Gänsicke B. T., Nebot Gómez-Morán A., 2010, A&A, 520, A86
Zorotovic M., Schreiber M. R., Gänsicke B. T., 2011a, A&A, 536, A42
Zorotovic M. et al., 2011b, A&A, 536, L3
Zorotovic M., Schreiber M. R., García-Berro E., Camacho J., Torres S., Rebassa-Mansergas A., Gänsicke B. T., 2014, A&A, 568, A68

APPENDIX A: OBSERVATIONAL SAMPLE

Table A1. Sample of detached WD+MS systems with M4–M6 companions used in this work. Systems in the period gap are highlighted in boldface. The sixth column details how the close binary nature and period was determined with the following meaning: RV – found via RV variations, period measured from velocities; RV > ELL – found via RV variations, period measured from ellipsoidal/reflection; RV > ECL – found via RV variations, period measured from eclipses; ECL – found via eclipses, period measured from eclipses. References: (1) Rebassa-Mansergas et al. (2008), (2) Rebassa-Mansergas et al. (2012), (3) Pyrzas et al. (2009), (4) Parsons et al. (2012b), (5) Nebot Gómez-Morán et al. (2011), (6) Parsons et al. (2013b), (7) Drake et al. (2010), (8) Parsons et al. (2013a), (9) Parsons et al. (2015), (10) Schreiber et al. (2008), (11) this paper, (12) Pyrzas et al. (2012), (13) Nebot Gómez-Morán et al. (2009), (14) Parsons et al. (2012a), and (15) Green, Richstone & Schmidt (1978).

System	P_{orb} (h)	Sp2	T_{eff} (K)	M_{WD} ($M_\odot$)	Method	References
SDSS J005245.11−005337.2	**2.735(2)**	**4.0**	**16 340 ± 4240**	**1.260 ± 0.365**	**RV**	**1,2**
SDSS J011009.09+132616.1	7.984 495(3)	4.0	25 167 ± 296	0.430 ± 0.015	RV > ECL	3,2
SDSS J013851.54−001621.6	1.746 3576(5)	5.0	3570^{+110}_{-80}	0.529 ± 0.010	ECL	4
SDSS J015225.38−005808.5	**2.151 95(1)**	**6.0**	**8773 ± 25**	**0.560 ± 0.059**	**RV**	**5**
SDSS J030308.36+005443.7	3.226 505(1)	4.5	<8000	0.910 ± 0.030	RV > ECL	3,6
SDSS J031404.98−011136.6	6.32(2)	4.0	–	0.650 ± 0.100	RV	1
SDSS J032038.72−063822.9	3.375(2)	5.0	11 264 ± 361	0.650 ± 0.158	RV	5
SDSS J083354.84+070240.1	7.34(2)	4.0	15 246 ± 560	0.540 ± 0.070	RV	5
SDSS J083845.86+191416.5	**3.122 694(9)**	**5.0**	**13 904 ± 424**	**0.390 ± 0.035**	**ECL**	**7,2**
SDSS J090812.04+060421.2	3.586 52(6)	4.0	17 505 ± 242	0.370 ± 0.018	ECL	7,2
SDSS J093947.95+325807.3	7.943 750(5)	4.0	28 398 ± 278	0.520 ± 0.026	ECL	7,2
SDSS J094634.49+203003.4	6.068 669 268(1)	5.0	10 268 ± 141	0.470 ± 0.098	ECL	8,2
SDSS J094913.37+032254.5	9.49(2)	4.0	18 542 ± 737	0.510 ± 0.079	RV	5
SDSS J101356.32+272410.6	**3.096 9691(1)**	**4.0**	**16 526 ± 277**	**1.100 ± 0.023**	**ECL**	**9,2**
SDSS J102102.25+174439.9	3.368 617 752(2)	4.0	32 595 ± 928	0.500 ± 0.050	ECL	8,2
SDSS J104738.24+052320.3	9.17(2)	5.0	12 392 ± 1715	0.380 ± 0.179	RV	10,2
SDSS J105756.93+130703.5	**3.003 890 76(1)**	**5.0**	**12 536 ± 978**	**0.340 ± 0.072**	**ECL**	**8,2**
SDSS J111459.93+092411.0	5.046 0816(2)	5.0	10 324 ± 172	0.610 ± 0.115	RV	11,2
SDSS J113006.11−064715.9	7.404 10(2)	5.0	11 139 ± 192	0.520 ± 0.076	RV	11,2
SDSS J114312.57+000926.5	9.27(3)	4.0	16 719 ± 534	0.523 ± 0.065	RV	5
SDSS J115156.94−000725.4	3.399(3)	6.0	10 395 ± 114	0.460 ± 0.095	RV	1,2
SDSS J121010.13+334722.9	**2.987 754 34(2)**	**5.0**	**6000 ± 200**	**0.415 ± 0.010**	**RV > ECL**	**12**

Table A1 – *continued*

System	P_{orb} (h)	Sp2	T_{eff} (K)	M_{WD} ($M_\odot$)	Method	References
SDSS J121258.25−012310.2	8.060 89(1)	4.0	17 707 ± 35	0.439 ± 0.02	ECL	13,14
SDSS J122339.61−005631.1	**2.161 8720(3)**	**5.5**	**12 166 ± 114**	**0.400 ± 0.043**	**ECL**	**8,2**
SDSS J123139.80−031000.3	5.849(9)	4.0	20 331 ± 1173	0.350 ± 0.068	RV	5
SDSS J124432.25+101710.8	5.468 549(5)	4.0	21 535 ± 435	0.400 ± 0.026	ECL	7,2
SDSS J130012.49+190857.4	7.39(1)	4.0	8657 ± 121	0.960 ± 0.103	RV	5
SDSS J130733.49+215636.7	5.191 731 1728(2)	4.0	–	–	ECL	8,2
SDSS J134841.61+183410.5	5.962(1)	4.0	15 071 ± 167	0.590 ± 0.017	RV	5
SDSS J140847.14+295044.9	4.602 966 48(1)	5.0	29 050 ± 484	0.490 ± 0.043	ECL	8,2
SDSS J141536.40+011718.2	8.263 939 986(2)	4.5	55 995 ± 673	0.564 ± 0.014	ECL	15,14
SDSS J142355.06+240924.3	9.168 10(4)	5.0	32 595 ± 318	0.410 ± 0.024	ECL	7,2
SDSS J143017.22−024034.1	4.353 8160(7)	5.0	10 802 ± 436	0.640 ± 0.201	RV	11,2
SDSS J143547.87+373338.5	**3.015 144(2)**	**5.0**	**12 392 ± 328**	**0.400 ± 0.038**	**RV > ECL**	**3,2**
SDSS J145238.12+204511.9	**2.549 2327(7)**	**4.0**	**–**	**≥0.89 ±**	**RV**	**11**
SDSS J145634.30+161137.7	5.498 885(5)	6.0	19 416 ± 262	0.370 ± 0.016	ECL	7,2
SDSS J152933.25+002031.2	3.962(3)	5.0	13 986 ± 368	0.385 ± 0.032	RV	1,2
SDSS J154846.00+405728.8	4.452 4258(4)	6.0	11 601 ± 349	0.510 ± 0.127	RV > ECL	3,2
SDSS J160821.47+085149.9	9.94(3)	6.0	9794 ± 130	0.800 ± 0.083	RV	5
SDSS J161113.13+464044.2	1.9768(5)	5.0	10 268 ± 60	0.480 ± 0.056	RV > ELL	5
SDSS J161145.88+010327.8	7.292(6)	6.0	10 159 ± 113	0.380 ± 0.096	RV	5
SDSS J162552.91+640024.9	5.237 71(5)	6.0	8779 ± 76	0.630 ± 0.096	RV	5
SDSS J173101.49+623315.9	6.433(6)	4.0	16 159 ± 548	0.410 ± 0.054	RV	5
SDSS J184412.58+412029.4	5.417(1)	6.0	7575 ± 6	0.290 ± 0.021	RV	5
SDSS J211205.31+101427.9	**2.2152(1)**	**6.0**	**19 868 ± 489**	**1.060 ± 0.051**	**RV > ELL**	**5**
SDSS J212320.74+002455.5	3.584(7)	6.0	13 432 ± 928	0.310 ± 0.066	RV	5
SDSS J213218.11+003158.8	5.334(3)	4.0	16 336 ± 303	0.390 ± 0.029	RV	5
SDSS J220848.32+003704.6	**2.4804(2)**	**5.0**	**–**	**≥0.33 ±**	**RV**	**11**
SDSS J221616.59+010205.6	5.049(5)	5.0	12 536 ± 1541	0.410 ± 0.143	RV	5
SDSS J223530.61+142855.0	3.466 955 6448(7)	4.0	21 045 ± 711	0.450 ± 0.055	ECL	8,2
SDSS J224038.37−093541.4	6.254(3)	5.0	13 300 ± 686	0.410 ± 0.049	RV	5
SDSS J224307.59+312239.1	**2.870(6)**	**5.0**	**–**	**–**	**RV > ELL**	**5**

This paper has been typeset from a TEX/LATEX file prepared by the author.